Troponin I Encompasses an Extended Troponin C in the Ca^{2+}-Bound Complex: A Small-Angle X-ray and Neutron Scattering Study†

Glenn A. Olah,‡ Sue E. Rokop,‡ C.-L. Albert Wang,§ Steven L. Blechner,‡,∥ and Jill Trewhella*,‡

Chemical Science and Technology Division, Los Alamos National Laboratory, Los Alamos, New Mexico 87545, and Boston Biomedical Research Institute, 20 Stanford Street, Boston, Massachusetts 02114

Received February 7, 1994; Revised Manuscript Received May 4, 1994®

ABSTRACT: We have studied the solution structure of skeletal muscle troponin C complexed with troponin I in the presence of calcium using small-angle X-ray and neutron scattering. $4Ca^{2+}$·troponin C in the complex has an extended dumbbell shape with a radius of gyration of 23.9 ± 0.5 Å and a maximum linear dimension of ≈72 Å, similar to the values obtained from the crystal structure coordinates of troponin C (Herzberg & James, 1985). Troponin I is even more extended than troponin C with a radius of gyration of 41 ± 2 Å and a maximum linear dimension of ≈118 Å. The centers-of-mass for each component of the complex are approximately coincident (<10-Å separation) as are their long axes, and the troponin I component encompasses the $4Ca^{2+}$·troponin C. These data provide new insights into the nature of the conformational arrangement of this important Ca^{2+}-sensitive molecular switch.

In the sliding-filament model of muscle action, thin and thick filaments move past each other, causing contraction or relaxation. The contractile force is believed to be generated by the cyclic attachment and detachment of the myosin heads of the thick filaments to sites on the thin filaments [for reviews, see Leavis and Gergely (1984) and Zot and Potter (1987)]. The thin filaments are composed of a double-stranded helical assembly of actin monomers. Tropomyosin is polymerized head-to-tail in the grooves of the thin filament actin helix (one tropomyosin to every seven actin monomers), and each tropomyosin has one troponin complex bound to it. The troponin complex has three subunits: troponin C (TnC)[1] which binds Ca^{2+}; troponin I (TnI); and troponin T (TnT). The regulation of the contraction/relaxation cycle is associated with an increase in calcium concentration and is mediated through the TnC component of the troponin complex. When TnC binds $4Ca^{2+}$, a signal is transmitted via TnI which releases its inhibition of the actin/myosin interaction via TnT and tropomyosin. Thus, the interactions of the thick and thin filaments are modulated to give rise to the sliding mechanism.

Low-resolution X-ray crystallographic and electron micrograph data of the troponin complex bound to tropomyosin show it to have an elongated shape with TnC and TnI forming a globular domain while TnT forms a long (≈160 Å) tail which interacts with tropomyosin (Flicker *et al.*, 1982; White *et al.*, 1987). The only high-resolution structural data on the components are for TnC. The crystal structures of TnC (Herzberg & James, 1985; Sundaralingam *et al.*, 1985) show this component to have an unusual dumbbell shape similar to the evolutionarily related calcium binding protein calmodulin (Babu *et al.*, 1985). These dumbbell structures consist of two globular domains connected by a solvent-exposed helix of approximately 7–8 turns. The C-terminal domain of TnC contains two high-affinity Ca^{2+}/Mg^{2+} binding sites, believed to be always occupied in muscle, while the N-terminal domain contains two lower-affinity Ca^{+}-specific binding sites. Both the high- and low-affinity binding domains have the helix–loop–helix secondary structure known as an EF-hand [Kretsinger, 1980; review by Wylie and Vanaman (1988)]. It is Ca^{2+} binding to the N-terminal domain that regulates the contractile event via a conformational change probably involving the opening of that "cup-shaped" domain, exposing hydrophobic residues on the inner surface of the cup (Herzberg *et al.*, 1986).

We have completed small-angle X-ray and neutron scattering experiments on $4Ca^{2+}$·TnC complexed with TnI in order to determine structural information such as the radius of gyration (R_g), the pairwise distribution function [$P(r)$], and the maximum linear dimension (d_{max}) for the overall complex and its components. The intensity of the scattering from a particle in solution depends upon its "contrast", i.e., the difference in scattering density between the particle and the solvent. X-rays are scattered by electrons, and the mean electron densities for most proteins are very similar. X-ray scattering thus gives information on the overall $4Ca^{2+}$·TnC·TnI complex. Neutrons are scattered by atomic nuclei, and hence isotopes of the same element can scatter neutrons quite differently. One of the largest differences is for hydrogen and deuterium. Thus, selective deuteration of one component in a complex, in this study TnC, provides a way of altering the neutron scattering density of that component. Further, by changing the deuterium level in the solvent, the neutron scattering contrast of each component is varied. If internal scattering density fluctuations are negligible, then "solvent

† This work was performed under the auspices of the DOE (Contract W-7405-ENG-36) and supported in part by an appointment of G.A.O. to the Alexander Hollaender Distinguished Postdoctoral Fellowship Program sponsored by DOE, Office of Health and Environmental Research, and administered by the Oak Ridge Institute for Science and Education. It was also supported in part by DOE/OHER Project KP-04-01-00-0 (J.T.), NIH Grant GM40528 (J.T.), and NIH Grant HL41411 (C.-L.A.W.). This work benefited from the use of facilities at the Manuel Lujan Jr. Neutron Scattering Center, a national user facility funded as such by DOE/Office of Basic Energy Sciences. This work also benefited from support by the National Science Foundation under Agreement DMR-9122444. We also acknowledge the support of the National Institute of Standards and Technology, U.S. Department of Commerce, in providing facilities used in the experiments.

* To whom correspondence should be addressed.

‡ Los Alamos National Laboratory.

§ Boston Biomedical Research Institute.

∥ Present address: Molecular Computing Facility, Beth Israel Hospital, Boston, MA 02215.

® Abstract published in *Advance ACS Abstracts,* June 15, 1994.

[1] Abbreviations: A_{600}, absorbance at 600 nm; CaM, calmodulin; D, centers-of-mass separation; d_{max}, maximum linear dimension; R_g, radius of gyration; R_c, radius of gyration of cross section; TnC, troponin C; $TnC_{78\%d}$, 78% deuterated troponin C; TnI, troponin I.

0006-2960/94/0433-8233$04.50/0

matching" can be achieved by adjusting the deuteration level in the solvent so that the mean solvent and particle scattering densities are the same; i.e., there is zero contrast and hence no small-angle scattering from the particle rendering it "invisible" in the neutron experiment. "Contrast variation" techniques thus provide methods for extracting structural information on the individual components as well as their relative dispositions (Ibel *et al.*, 1975; Moore, 1981).

MATERIALS AND METHODS

Sample Preparation. The neutron scattering experiment involved measuring a "contrast series" in which a complex of deuterated $4Ca^{2+}$·TnC and nondeuterated TnI is solubilized in solvents with different D_2O:H_2O ratios. Partial deuteration of the TnC component was chosen in order to have the solvent match point for the overall complex between 65 and 72% D_2O, thus allowing neutron scattering measurements on either side of the solvent match point.

Partially deuterated TnC was produced using a bacterial expression system obtained from S. Hitchcock-DeGregori (University of Medicine and Dentistry of New Jersey, Robert Wood Johnson Medical School). The TnC gene is in a pET 3d vector in *Escherichia coli* BL21(DE53)plysS. The cells were grown in 75–80% D_2O using M9 salts with an organic supplement containing deuterated and nondeuterated components. The deuterated organic components came from Merck deuterated whole algal hydrolysate, reported by Merck to be 60–65% amino acids, 10–15% sugars, and 30–35% salts. The amino acid composition of the hydrolysate was determined by amino acid analysis. The hydrolysate was diluted with nondeuterated amino acids and glucose to give a 3:1 ratio of deuterated to nondeuterated amino acids and sugars. The final organic supplement was 10 g/L. The media also contained 20 mg/L ampicillin and 25 mg/L chloramphenicol. Cells were grown at 37 °C to an A_{600} of 0.4 in a BioFlo II fermentor (New Brunswick Scientific). TnC expression was induced by addition of IPTG to a concentration of 0.4 mM. Growth was monitored at A_{600} until it leveled off, usually at about A_{600} = 2.4 after 3–4 h. Cells were harvested by centrifugation in a Beckman J21C with a J-14 rotor for 15 min at 12 000 rpm, and the pellet was frozen overnight at −80 °C.

TnC was purified according the method of Xu and Hitchcock-Degregori (1988) with several modifications. The ammonium sulfate fractionation they describe was always carried out, followed by the phenyl-Sepharose column and HPLC separation steps. The phenyl-Sepharose fractions were combined and dialyzed against 0.001 M NH_4HCO_3 to remove salts, and the dialysate was lyophilized. The lyophilized powder was resuspended in 20 mM sodium phosphate buffer, pH 6.5, 0.1 mM $CaCl_2$, and applied to a Pharmacia ProRPC HR 5/10 reverse-phase HPLC column. After the column was washed with the same buffer, a linear gradient was applied: 20 mM sodium phosphate, pH 6.5, 0.1 mM $CaCl_2$ going to 50% of 20 mM sodium phosphate with 50% acetonitrile, in 50 min and 0.3 mL/min. The TnC fractions were lyophilized to remove the acetonitrile, taken up in minimal water, dialyzed against 0.1 mM NH_4NCO_3 to remove salts, and lyophilized. The purity of the final product (typically >99%) was verified via SDS gel electrophoresis.

NMR spectroscopy was used to determine the degree of deuteration of the TnC by measuring the amino acid proton signal in an ultrapure D_2O (99.996% D) phosphate buffer. The hydrogens of Na_2HPO_4 and NaH_2PO_4 were exchanged with deuterium by repeated dissolution in D_2O and lyophilization. A stock buffer solution was prepared by mixing Na_2DPO_4 and NaD_2PO_4 at a ratio to give a pH reading of 6.52 and 50 mM phosphate. Approximately 400 μL of this stock solution was used to dissolve TnC which was added as a dry powder. The deuteration level was determined by comparing the integrated proton signal amplitudes of the partially deuterated TnC sample with that of a nondeuterated TnC sample, both of known protein concentrations (≈3.5 mM). The deuteration level for the TnC was determined to be 78 ± 1% for the nonexchangeable hydrogens. By comparison with a previous neutron scattering study of calmodulin (Trewhella *et al.*, 1990) and analysis of the present neutron scattering study, it was determined that approximately 45% of the exchangeable hydrogens readily exchange and it was assumed that this H/D exchange was linear with the deuterium content of the solvent.

Nondeuterated TnI was prepared by the method of Wilkinson and Grand (1975, 1978). Similar to TnC, it is assumed that 45% of the exchangeable hydrogens exchanged linearly with the deuterium content of the solvent.

$TnC_{78\%d}$ and TnI were completed by dissolving the appropriate quantity of each protein (in a 1:1 stoichiometry) in 0.5 mL of a 6 M urea solution. This solution was dialyzed against buffer A with 2 or 3 M urea (buffer A: 50 mM MES, 2 mM $CaCl_2$, 1 mM DTT, and 100 mM KCl, pH 6.1). The calcium was in ≈20 times stoichiometric excess of the TnC. Dialysis was repeated 4 times against buffer A with 0%, 40%, or 100% D_2O. The last dialysate buffer was saved and used for solvent scattering measurements. The 20% D_2O sample was made by mixing the appropriate amount of the 0% and 40% D_2O samples. Similarly, the 90% D_2O was prepared from the 0% and 100% D_2O samples. pH values measured for samples in 100% D_2O were adjusted by subtracting 0.4 pH unit. Initially, samples prepared in D_2O buffer without urea showed D_2O-induced aggregation of the complex. This aggregation was eliminated by working with low protein concentrations (1–4 mg/mL) in buffer A with 2 or 3 M urea. It is known that TnC complexed with TnI forms a stable complex under saturating Ca^{2+} conditions even in the presence of 6 M urea (Grabarek *et al.*, 1981). In the buffer composition used, the solvent match points were calculated from the chemical compositions of the components as 42% D_2O for TnI and 101% D_2O for $4Ca^{2+}$·$TnC_{78\%d}$. The solvent match point for the overall complex was calculated as 71% D_2O.

Scattering Data Acquisition and Reduction. All scattering data were reduced to $I(Q)$ versus Q, where $I(Q)$ is the scattered neutron or X-ray intensity and Q is the amplitude of the scattering vector. Q is equal to $4\pi \sin \theta/\lambda$, where 2θ is the scattering angle and λ is the wavelength of the incident and scattered neutrons or X-rays.

Small-angle neutron scattering (SANS) measurements were done using the low-Q-diffractometer (LQD) at the Manuel Lujan Jr. Scattering Center (LANSCE) (Seeger *et al.*, 1990) and the 30 m SANS instrument (NG3) at the National Institute of Standards and Technology (NIST). The neutrons at LANSCE are produced by a spallation source which is pulsed, and hence a range of wavelengths can be used with time-of-flight methods, allowing measurement of a large Q range with a single detector position. The Q range measured using LQD was 0.005–0.35 $Å^{-1}$. $4Ca^{2+}$·$TnC_{78\%d}$·TnI samples (2–4 mg/mL) in buffer A with 2 M urea in 0%, 40%, and 100% D_2O and a $4Ca^{2+}$·$TnC_{78\%d}$·TnI (1.5–3.0 mg/mL) sample in buffer A with 3 M urea in 100% D_2O were measured. The 30 m SANS instrument at NIST uses neutrons produced by a 20 MW reactor from which we selected neutrons with a mean wavelength of 5.0 Å and a full width and half-maximum of 34%. Sample-to-detector distances of 7 and 1.5 m were

used in order to cover the appropriate Q range (0.01–0.08 and 0.04–0.3 Å^{-1}, respectively). $4Ca^{2+}$·$TnC_{78\%d}$·TnI samples in buffer A with 2 M urea in 0%, 20%, and 40% D_2O (2–4 mg/mL) and $4Ca^{2+}$·$TnC_{78\%d}$·TnI samples in buffer A with 3 M urea in 90% and 100% D_2O (1.5–2.5 mg/mL) were measured. With 2 or 3 M urea present, the solvent density increased a few percent (2–6%), which was taken into account in the data reduction and analysis. Quartz cuvettes with 1-mm path lengths were used for the 0%, 20%, and 40% D_2O samples. Since the neutron transmissions for the 90% and 100% D_2O samples were higher due to their lower hydrogen content, 2- and 3-mm path-length quartz cuvettes were used for these samples, respectively. Measurements at both neutron scattering facilities were reduced by standard techniques used for buffer subtraction and detector sensitivity corrections (Chen & Bendedouch, 1986; Crawford *et al.*, 1987; Hjelm, 1988; Seeger *et al.*, 1990).

X-ray scattering data were collected using the small-angle X-ray scattering (SAXS) station at Los Alamos which is described elsewhere (Heidorn & Trewhella, 1988; Olah *et al.*, 1993). The sample-to-detector distance was 64 cm. Concentration series of the complex in H_2O for two different sample preparations in buffer A were performed and showed that interparticle interference is negligible over the concentration range used in the neutron scattering experiments (1.5–4 mg/mL). X-ray scattering measurements were also made on each sample used in the neutron scattering study before and after the neutron measurements to check for aggregation and structural integrity.

Scattering Data Analysis. The scattering from a homogeneous solution of monodisperse particles can be expressed as

$$I(Q) = |\int [\rho(r) - \rho_s] \exp[-i(Q\cdot r)\, dr]|^2 \quad (1)$$

where $\rho(r)$ and ρ_s are the scattering density for the protein and solvent, respectively, and the integration is taken over the volume of the protein. If we ignore scattering density fluctuations and treat the $4Ca^{2+}$·TnC·TnI complex as a two-component system, we can write the scattering as

$$I(Q,\Delta\rho_C,\Delta\rho_I) = \Delta\rho_C{}^2 I_C(Q) + \Delta\rho_C\Delta\rho_I I_{CI}(Q) + \Delta\rho_I{}^2 I_I(Q) \quad (2)$$

where the subscripts C and I refer to TnC and TnI. $\Delta\rho_C$ equals $\rho_C - \rho_s$ where ρ_C is the mean scattering density for $4Ca^{2+}$·TnC. A similar definition holds for $\Delta\rho_I$. The three terms in eq 2 correspond to the three basic scattering functions. $I_C(Q)$ and $I_I(Q)$ represent the scattering of $4Ca^{2+}$·TnC and TnI in the complex, respectively, while $I_{CI}(Q)$ is a cross-term. Each scattering measurement at a given D_2O:H_2O ratio of the solvent (total of nine independent measurements at five different D_2O:H_2O ratios) gives an equation in the form of eq 2; thus, a multiple linear regression routine was written to solve this overdefined system of equations for the three basic scattering functions. The scattering densities, $\Delta\rho_C$ and $\Delta\rho_I$, are readily calculated from chemical and isotope compositions of the two components of the complex and the solvent. The inverse Fourier transform of $I(Q)$ gives the vector distribution function, $P(r)$, which is the frequency of all interatomic vectors within the scattering particle and hence goes to zero at d_{max}. The first and second moments of $P(r)$ give the zero angle scatter, I_0, and R_g of the particle, respectively.

For a two-component system, the square of R_g can be expressed as

$$R_g{}^2 = f_C'R_C{}^2 + f_I'R_I{}^2 + f_C'f_I'D^2 \quad (3)$$

where

$$f_C' = \Delta\rho_C V_C/(\Delta\rho_C V_C + \Delta\rho_I V_I)$$

$f_I' = 1 - f_C'$. Equation 3 is the "parallel axis theorem" for a two-component system (Moore, 1981). R_C and R_I are the R_g's for each component, and D is the separation of the centers-of-mass of the components. The volumes of each component, V_C and V_I, can be estimated from their molecular weights assuming a protein specific volume of 0.72 cm^3/g. f_C' and f_C' are also readily calculated from the chemical and isotope composition of each component. R_C, R_I, and D can be calculated from eq 3 using a multiple linear regression routine.

Ibel and Stuhrmann (1975) showed that the $R_g{}^2$ dependence on the scattering contrast can be written in another form as

$$R_g{}^2 = R_m{}^2 + \alpha/\Delta\bar{\rho} - \beta/\Delta\bar{\rho}^2 \quad (4)$$

where R_m is the R_g at infinite contrast and $\Delta\bar{\rho} \equiv \bar{\rho} - \rho_s$, where $\bar{\rho}$ is the mean scattering density for the total particle and ρ_s is the scattering density of the solvent. The coefficient α is related to the second moment of the scattering density fluctuations about the mean value for the scattering particle, while β is related to the square of the first moment of the density fluctuations about the mean. For a two-component system, R_m, α, and β can be expressed as

$$R_m{}^2 = f_C R_C{}^2 + f_I R_I{}^2 + f_C f_I D^2 \quad (5a)$$

$$\alpha = (\rho_C - \rho_I) f_C f_I [R_C{}^2 - R_I{}^2 + (f_I{}^2 - f_C{}^2)D^2] \quad (5b)$$

$$\beta = (\rho_C - \rho_I)^2 f_C{}^2 f_I{}^2 D^2 \quad (5c)$$

where

$$f_C = V_C/(V_C + V_I)$$

$$f_I = 1 - f_C$$

R_m, α, and β can be determined from eq 4 using a polynomial least-squares fit of $R_g{}^2$ versus $1/\Delta\bar{\rho}$. If the sign of α is positive, then the lower scattering density component (in this case the TnI) is located more toward the inside of the complex than the higher scattering density component (the partially deuterated TnC). A negative α indicates the reverse case. β is proportional to the square of the separation of the two components. If β is zero, then the centers-of-mass are coincident. Once R_m, and α, and β are determined, the three linear eqs 5 can be solved for R_C, R_I, and D.

The measured scattering data are "smeared" as a result of the finite wavelength distribution and beam shape of the incident radiation. To correct for these effects, all intensity curves were individually analyzed using the indirect Fourier transform algorithm described by Moore (1980). This algorithm models the intensity curves, $I(Q)$, by calculating the pair-distance, or vector distribution function, for a homogeneous scattering particle, $P(r)$. The $P(r)$ function is determined by setting $P(r)/r$ to zero at $r = 0$ and at some maximum dimension, d_{max}, and representing it as a sine series. The number of terms in the sine series is limited by $d_{max}Q_{max}/\pi$, where Q_{max} is the maximum Q of the experiment. The smearing effects due to the wavelength distribution and beam shape can be incorporated into the coefficients of the sine series from which the corresponding unsmeared $I(Q)$, used in the analyses described by eqs 1–5, can be calculated using a Fourier transform:

$$I(Q) = 4\pi \int P(r) \sin(Q\cdot r)/(Q\cdot r)\, dr \quad (6)$$

RESULTS

X-ray scattering data for $4Ca^{2+}$·$TnC_{78\%d}$·TnI are shown in Figure 1, with the corresponding $P(r)$ function in Figure 4(top).

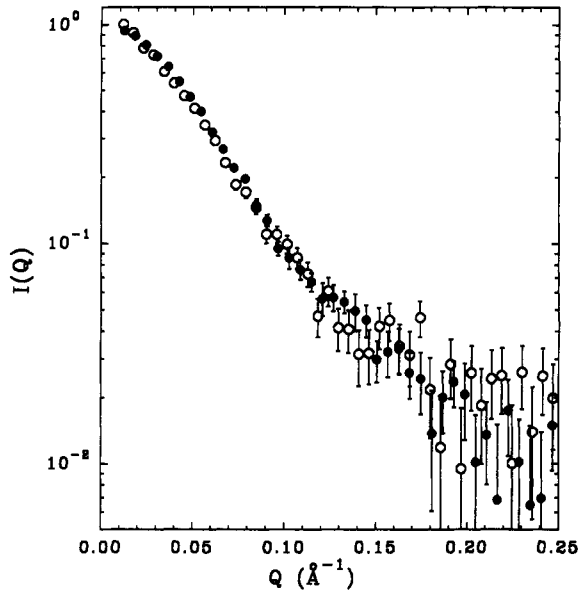

FIGURE 1: Comparison of X-ray scattering data from the $4Ca^{2+}$·$TnC_{78\%d}$·TnI complex, ≈3 mg/mL protein, in buffer A (○) with H_2O and 0 M urea and (●) in buffer A with D_2O and 3 M urea.

Since TnC and TnI have approximately equal X-ray scattering densities, the scattering curve and $P(r)$ profile correspond to those for the overall complex. The $P(r)$ function is asymmetric, showing a broad peak at ≈38 Å with a tail extending to ≈115 Å, indicating the complex itself is asymmetric. Indeed, Guinier analysis for "rod"-shaped particles [reviewed in Glatter (1982)] shows the complex to be elongated with an average radius of cross section, R_c, of 16.2 ± 1.5 Å (Figure 3, bottom, and Table 2).

$4Ca^{2+}$·TnC·TnI in H_2O is monodisperse for concentrations less than 5 mg/mL. This was determined by measuring the forward scatter, I_0, which is directly proportional to the molecular weight of the scattering species and comparing with a standard protein (lysozyme) known to be monodisperse (Kringbaum & Kugler, 1970). Initial attempts to measure scattering data from samples in D_2O, however, showed the complex to have a tendency to aggregate in solutions with >20% D_2O. D_2O-induced aggregation often arises from hydrophobic interactions which can sometimes be disrupted by adding mild denaturants. We therefore added urea or guanidine thiocyanate with concentrations between 0.5 and 3 M. We also tried using 10–40% (v/v) glycerol, as well as varying the complex concentration from 1.5 to 7 mg/mL. X-ray scattering data measured for samples under these various conditions were compared with the scattering data for monodisperse samples in H_2O in order to evaluate aggregation. 2–3 M urea proved the most effective agent for eliminating aggregation without affecting the structure of the complex as determined from the scattering data. A comparison of the X-ray scattering profiles for the complex in buffer A using H_2O with no urea and using D_2O with 3 M urea is given in Figure 1. The profiles are identical in the Q range used for analysis (0.015–0.25 Å^{-1}). Samples in buffer A with 2 M urea also gave the same profile over this Q range. The difference between the mean scattering solvent density for samples in buffer A with 2 or 3 urea was negligible. Therefore, X-ray scattering data taken for samples with 2 and 3 M urea, a total of nine separate measurements, were combined to give a final X-ray scattering profile with improved statistics for the structural analysis.

The neutron scattering profiles for $4Ca^{2+}$·$TnC_{78\%d}$·TnI samples measured at NIST are given in Figure 2. The data are not normalized with respect to concentration or path length

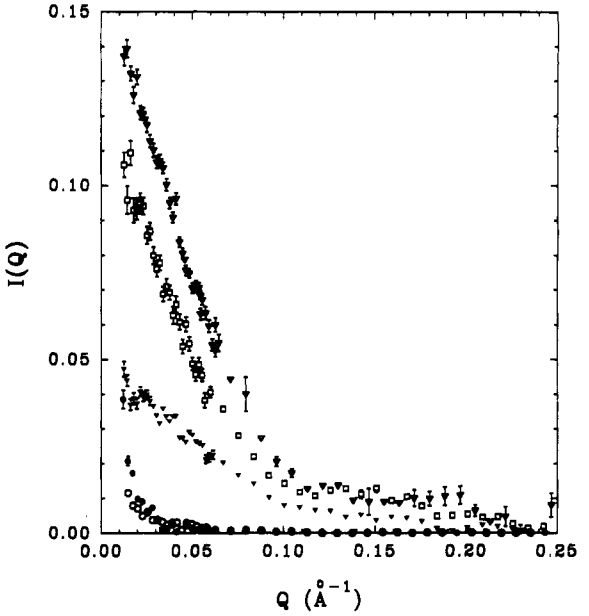

FIGURE 2: Neutron scattering data for $4Ca^{2+}$·$TnC_{78\%d}$·TnI collected on beamline NG3 at NIST with (▽) 0%, (□) 20%, (▼) 40%, (●) 90%, and (○) 100% D_2O. The 0%, 20%, and 40% D_2O samples contained 2 M urea, and the 90% and 100% D_2O samples contained 3 M urea. Data are on the same arbitrary normalization scale, but not corrected for concentration or path-length differences.

Table 1: R_g Values from $P(r)$ Analysis of Neutron and X-ray Scattering Data

	% D_2O	[urea] (M)	R_g (Å)
neutron (NIST)			
JAN93	0	2	27.7 ± 0.5
JAN93	20	2	27.1 ± 0.5
JAN93	40	2	23.3 ± 0.5
SEP93	90	3	48.0 ± 4.0
SEP93	100	3	41.8 ± 2.0
neutron (LANSCE)			
SEP92	0	2	28.5 ± 2.0
SEP92	40	2	23.1 ± 1.2
SEP92[a]	100	2	44.0 ± 4.0
AUG93	100	3	42.5 ± 4.0
X-ray[b]			33.3 ± 0.8

[a] This data set showed no evidence of aggregation for $q > 0.027$ Å, and, therefore, it was used in the analyses. [b] From the X-ray scattering profile calculated by combining nine separate measurements as described under Results.

in order to show the differences in intensity of the raw data between samples. The results from the measurements of LANSCE were consistent with the NIST data. Table 1 gives R_g values for the data collected at both facilities.

The basic scattering functions determined from eq 2 using nine neutron scattering data sets for five different D_2O:H_2O ratios plus the combined X-ray scattering data set are shown in Figure 3. The basic scattering functions were quite robust; that is, they did not change in shape with the number of data sets included in the analysis down to the minimum required of three. Inclusion of more data sets simply improved statistics. The basic scattering function corresponding to the $4Ca^{2+}$·TnC component extends to larger scattering angle than that for the TnI component, indicating TnC is less extended than TnI. The scattering curve calculated from the crystal structure of TnC is also given in Figure 3, and it is in good agreement with the basic scattering function of $4Ca^{2+}$·TnC in scattering space. The inverse Fourier transform of the scattering curves for $4Ca^{2+}$·TnC and TnI in Figure 3 gives the $P(r)$ functions shown in the middle and bottom panels, respectively, of Figure 4. The $P(r)$ function of $4Ca^{2+}$·TnC is very similar to that expected

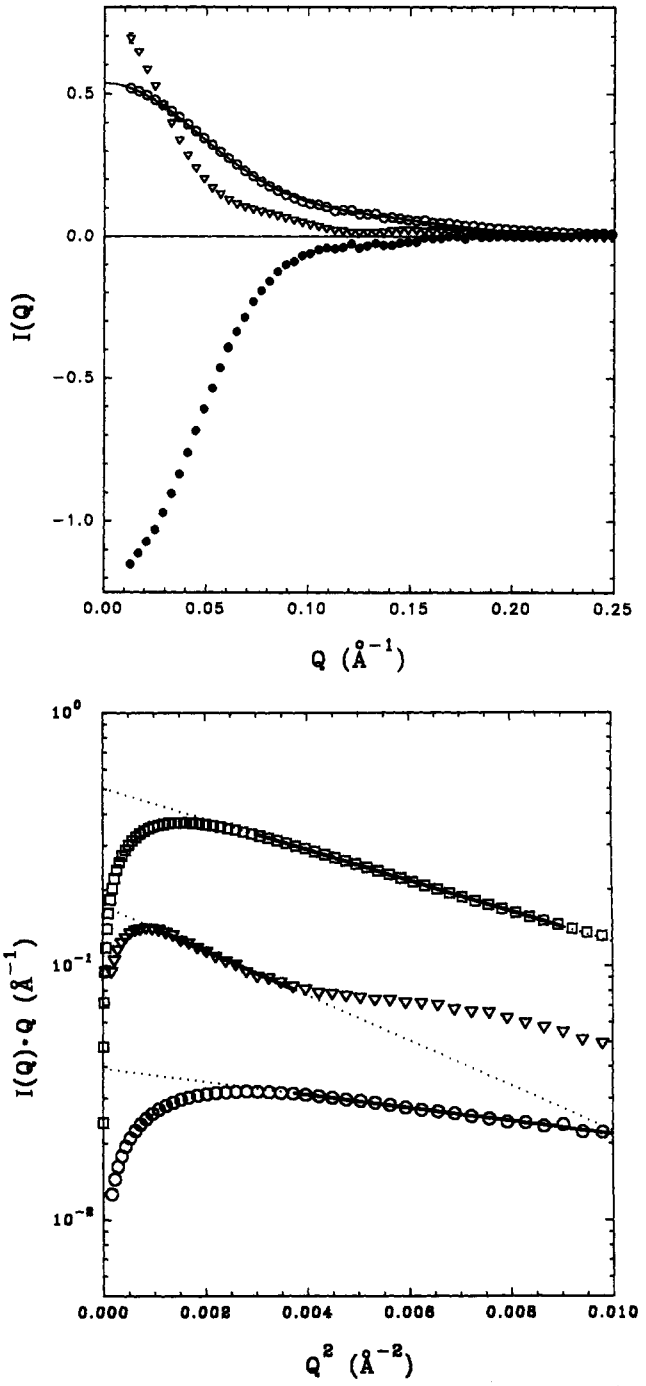

FIGURE 3: (Top) Basic scattering functions calculated using eq 2 for $4Ca^{2+}$·$TnC_{78\%d}$ (○), TnI (▽), and the cross-term (●) between the two proteins in the complex. The solid line is the calculated scattering curve from the known crystal structure of $2Ca^{2+}$·TnC (Herzberg & James, 1985). (Bottom) Guinier showed that for a "rod-shaped" particle, a plot of ln $I[(Q)\cdot Q]$ vs Q^2 is linear at certain small Q values, with a slope proportional to the mean R_c value of the scattering particle. Shown here are the Guinier plots for $4Ca^{2+}$·TnC (○) and TnI (▽) (using the basic scattering functions) and for $4Ca^{2+}$·TnC·TnI (□) (using the X-ray scattering data). The solid lines show the regions of the Guinier plots fitted for each profile, and the dotted lines are extrapolations of those fits. The roll-over observed at the lowest Q values is expected because of the finite lengths of the rod-shaped particles. The linearity is also expected to break down at high Q values, and the Q value at which this breakdown occurs is indirectly proportional to the R_c value (as we observe for these data sets).

for the crystal structure of $2Ca^{2+}$·TnC (Herzberg & James, 1985). It shows a peak at ≈18 Å, corresponding to the approximate radius of each of the globular lobes, and a secondary peak at ≈45 Å resulting from the separation of the two lobes. The $P(r)$ function calculated from the crystal

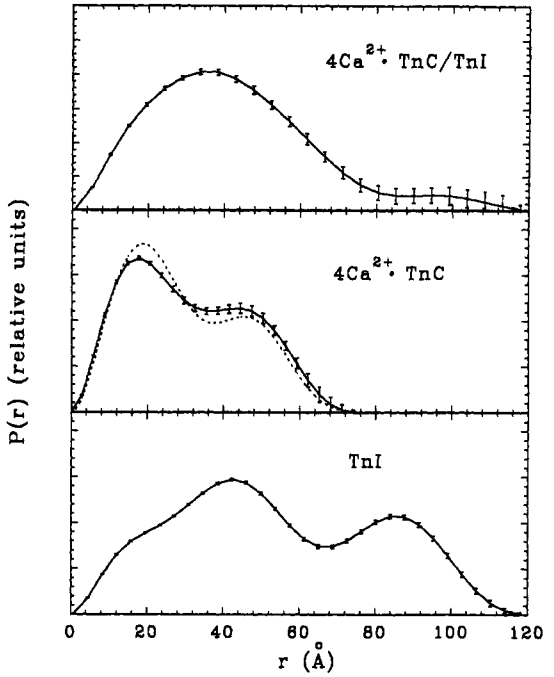

FIGURE 4: (Top) $P(r)$ function for $4Ca^{2+}$·$TnC_{78\%d}$·TnI determined from the X-ray scattering data. Middle and bottom panels are the $P(r)$ functions for $4Ca^{2+}$·$TnC_{78\%d}$ and TnI, respectively, as determined from the basic scattering functions given in Figure 3. The dotted line in the middle graph is the calculated $P(r)$ function from the crystal structure of TnC (Herzberg & James, 1985).

Table 2

	$4Ca^{2+}$·TnC[a]	TnI	$4Ca^{2+}$·TnC·TnI
R_g (Å) [and d_{max} (Å)] Values Derived from Three Methods of Analysis			
basic scattering functions	23.9 ± 0.5	41.2 ± 2.0	33.0 ± 0.5
	(72 ± 3)[b]	(118 ± 4)	(115 ± 4)
parallel axis theorem[c]	23.9 ± 0.4	41.6 ± 1.2	34.5 ± 1.0
Stuhrmann analysis[c]	23.5 ± 1.0	41.5 ± 2.0	32.7 ± 1.0
R_c (Å) Values Derived from Guinier Analysis of the Basic Scattering Functions			
	10.7 ± 1.0	20.5 ± 2.0	16.2 ± 1.5

[a] For comparison, $2Ca^{2+}$·TnC has an R_g of 23.9 Å and a d_{max} of 72 Å (Herzberg & James, 1985; Trewhella & Heidorn, 1988). [b] Values in parentheses are d_{max}. [c] The best fit gave values for the center-of-mass separation (D) are 0 ± 10 Å.

structure differs from that shown in Figure 4(middle) only in the relative amplitudes of these two peaks. The ratio of the peak at ≈18 Å to that at ≈45 Å is 20% greater for the crystal structure $P(r)$. The R_g and d_{max} values for $4Ca^{2+}$·TnC in the complex (Table 2) agree well with those calculated from the crystal structure coordinates. These data indicate that the interconnecting helix of TnC is extended when it is complexed with TnI, more like the crystal structure as compared with the solution structure in which the globular domains are on average closer together (Heidorn & Trewhella, 1988). The average R_c value for $4Ca^{2+}$·TnC is 10.7 ± 1.0 Å (Figure 3, bottom, Table 2).

The $P(r)$ function for TnI is even more extended than that for $4Ca^{2+}$·TnC. It shows two peaks, at ≈43 and 86 Å, and a shoulder at ≈10–20 Å. The shape and amplitudes of the two peaks cannot arise from a simple dumbbell shape like TnC. The R_c value for the TnI component is 20.5 Å (Figure 3, bottom, Table 2). A detailed modeling procedure based on a Monte Carlo method (Heidorn *et al.*, 1988) has been developed to model and test possible TnI structures (Olah and Trewhella, unpublished results).

A Stuhrmann plot (R_g^2 versus $1/\Delta\bar{\rho}$) is shown in Figure 5. The lines were calculated using eq 5 with R_g values determined

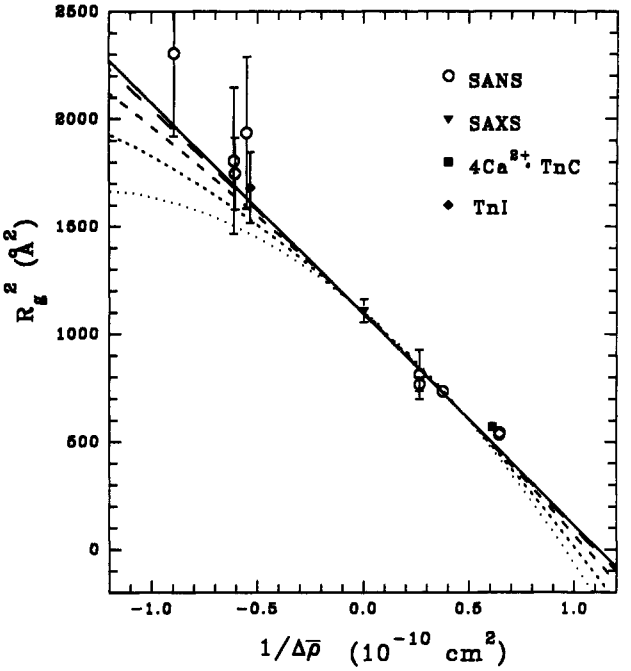

FIGURE 5: Stuhrmann plot (R_g^2 versus $1/\Delta\bar{\rho}$). The line fits were determined from eqs 4 and 5 by assuming fixed R_g values of 23.9 and 41 Å for 4Ca^{2+}·TnC and TnI, respectively, and varying the separation, D, of the two components. Separations are (–) 0, (– –) 5, (– –) 10, (- - -) 15, and (···) 20 Å.

from the basic scattering functions and assuming center-of-mass separations ranging from 0 to 20 Å. The scattering data exclude solutions for which the center-of-mass separation of the two components is >10 Å. The negative slope (α in eq 4) indicates that the component with the larger neutron scattering power (4Ca^{2+}·TnC$_{78\%d}$) is located more toward the center of the total complex. The R_g value calculated from the X-ray scattering data is approximately equivalent to scattering at infinite contrast and is also included in the Stuhrmann plot. R_C, R_I, and D resulting from solution of the Stuhrmann analysis (eqs 4 and 5) are given in Table 2. Also, in Table 2 are the structural parameters determined from the "parallel axis theorem" (eq 3) along with those determined from the basic scattering functions showing that the different methods of analysis are in excellent agreement.

The R_c values for the two components and the complex give information on the relative orientations of their long axes. In the limiting case in which 4Ca^{2+}·TnC is approximated as a simple rod shape surrounded by TnI approximated as a simple annular cylinder, with each component constrained to have their centers-of-mass coincident and long axes parallel, the R_c value for the total complex (R_{cT}) can be calculated using $R_{cT} = f_C R_{cC}^2 + f_I R_{cI}^2$ where $f_{I,C}$ are the mass fractions of each component and $R_{cC,I}$ are the respective R_c values. Substitution of R_c values for 4Ca^{2+}·TnC and TnI (Table 2) into this equation gives an R_{cT} value of 16.6 Å, in agreement with the measured value for the complex. Nonparallel axes would give increasingly larger R_{cT} values (up to 21 Å for the limit of perpendicular axes). Therefore, we conclude the long axes of 4Ca^{2+}·TnC and TnI (as well as that for the overall complex) are approximately coincident.

DISCUSSION

The neutron and X-ray scattering data presented here give the first view of the nature of the conformational interaction between 4Ca^{2+}·TnC and its regulatory target TnI. The data show 4Ca^{2+}·TnC in the complex is extended, similar to the crystal structure for 2Ca^{2+}·TnC, as determined from the R_g and d_{max} values and the $P(r)$ function. The small discrepancy in the relative amplitudes of the peaks in the $P(r)$ function determined from the basic scattering functions and that determined from the 2Ca^{2+}·TnC crystal structure coordinates could be attributed to Ca^{2+}-induced conformational changes such as the opening of the "cup"-shaped N-domain of 4Ca^{2+}·TnC (Herzberg et al., 1986). The basic conclusion that the TnC component in the complex is dumbbell-shaped and the connecting region between the two globular lobes is extended similar to the crystal structure remains firm. The TnI component is even more extended than 4Ca^{2+}·TnC, and the maximum linear dimensions of the TnI component and the overall complex (≈118 Å) are the same. The long axes of the two components are approximately coincident, as are their centers-of-mass, and the TnI component is more toward the outside of the complex encompasssing the 4Ca^{2+}·TnC.

An extended 4Ca^{2+}·TnC complexed with TnI is consistent with an earlier observation using energy transfer methods (Wang *et al.*, 1987). However, this is quite different from the current view of the interactions between the evolutionarily related calmodulin (CaM) and a number of its regulatory targets. Structural studies of 4Ca^{2+}·CaM complexed with synthetic peptides based upon binding domains from smooth muscle and skeletal muscle myosin light chain kinase (MLCK) (Heidorn *et al.*, 1989; Ikura *et al.*, 1992; Meador *et al.*, 1992, 1993) show CaM contracts around the short (≈20 residue) target sequence, which forms a bifurcated basic amphipathic α-helix, via flexibility in the "helical" sequence connecting the two globular lobes of CaM. Hydrophobic residues along the helical target sequence form tight interactions with the hydrophobic pockets on each of CaM's globular lobes. This mode of interaction has also been observed for a variety of peptide sequences, including a number that appear to have no physiological relevance but do form basic, amphipathic helices (Kataoka *et al.*, 1989, 1991; Yoshino *et al.*, 1989). Sequence analysis of a variety of Ca^{2+}·CaM-regulated enzymes indicates this may be a general feature of a number of targets (O'Neil & DeGrado, 1989). The target enzymes that share these CaM binding domain features generally only bind CaM in the presence of Ca^{2+}. In contrast, phosphorylase kinase is a multisubunit enzyme made up of a tetramer of tetramers, $(\alpha\beta\gamma\delta)_4$, and the δ-subunit is CaM which modulates the activity of the catalytic or γ-subunit in a Ca^{2+}-dependent manner [for a review, see Pickett-Giess and Walsh (1986)]. Like TnC in the troponin complex, CaM remains an integral part of phosphorylase kinase in the presence and absence of Ca^{2+}. The CaM binding region in the γ-subunit is distinct from other CaM binding domains in that it is made up of two noncontiguous subdomains that bind to CaM simultaneously (Dasgupta *et al.*, 1989). Further, Dasgupta *et al.* (1989) identified sequence similarities between the CaM binding subdomains and TnI. The regions of sequence similarity include a four-residue region of sequence identity that overlaps with the TnI inhibitory peptide sequence [TnI(104-115)] which is the shortest peptide segment needed to inhibit actin–myosin interaction and ATPase activity (Syska *et al.*, 1976; Talbot & Hodges, 1981; Van Eyk & Hodges, 1988). Small-angle X-ray and neutron scattering data on CaM complexed with the two CaM binding subdomains identified in the γ-subunit of phosphorylase kinase showed CaM to be extended (Trewhella *et al.*, 1990). Small-angle X-ray scattering experiments (Blechner *et al.*, 1992) on TnC complexed with a number of peptides, including the TnI inhibitory peptide sequence, showed TnC to be extended in its interaction with this peptide sequence, as well as with another TnC binding sequence, TnI(1–30), which has been suggested to act as a negative regulator of the

TnI inhibitory region (Ngai & Hodges, 1992). These observations led us to speculate (Trewhella *et al.*, 1990; Blechner *et al.*, 1992) that the interaction of TnC with TnI may be similar to the interaction between CaM and the γ-subunit of phosphorylase kinase. The data presented here support this speculation, and give further support to the idea that the extended TnC and CaM structures may be important in maintaining Ca^{2+}-independent associations in some systems.

Several studies have concluded that the TnI inhibitory peptide interacts with regions in both the C- and N-terminal domains of TnC [Farah *et al.*, 1994; for a review, see Ngai and Hodges (1992), Swenson and Frederickson (1992), and Kobayashi *et al.* (1991)]. Nuclear magnetic resonance (NMR) studies of the TnI inhibitory peptide sequence complexed with TnC in the presence of Ca^{2+} show it to form a one-turn amphiphilic α-helix which is distorted around two central prolines (Campbell & Sykes, 1991; Campbell *et al.*, 1992). This peptide structure would not be long enough to span the distance between the N- and C-terminal domains determined from the data presented here, indicating that the peptide could not simultaneously interact with both domains. Alternatively, one could consider the possibility that the inhibitory peptide has a propensity to interact independently with each domain since there is structural similarity between the two domains. This possibility has been suggested elsewhere (Ngai & Hodges, 1992; Swenson & Frederickson, 1992). Further, Ngai and Hodges (1992) showed that a subtle difference exists between the action of the TnI(1–40) regulatory peptide and the regulatory region of TnI when each binds to TnC. These observations suggest caution must be taken when interpreting results from studies utilizing peptides to model the interaction between TnC and TnI, and there may also be differences between the interaction with TnC of the TnI inhibitory peptide and the corresponding region in intact TnI.

ACKNOWLEDGMENT

We thank Philip A. Seeger (LANSCE) and Susan Krueger (NIST), who were our local contacts at their respective neutron scattering facilities, and who were helpful and hospitable for the many visits it took to gather the neutron data for this study. We also thank Donald K. Blumenthal for helpful discussions.

REFERENCES

Babu, Y. S., Buff, C. E., & Cook, W. J. (1988) *J. Mol. Biol. 204*, 191.
Campbell, A. P., & Sykes, B. D. (1991) *J. Mol. Biol. 222*, 405.
Campbell, A. P., Van Eyk, J. E., Hodges, R. S., & Sykes, B. D. (1992) *Biochim. Biophys. Acta 1160*, 35.
Chen, S.-H., & Bendedouch, D. (1986) in *Methods in Enzymology* (Hirs, C. H. W., & Timasheff, S. N., Eds.) pp 79–117, Academic Press, New York.
Crawford, R. K., Epperson, J. E., Thiyagarajan, P., & Trouw, F., Eds. (1987) IPNS Note 46.
Dasgupta, M., Honeycutt, T., & Blumenthal, D. K. (1989) *J. Biol. Chem. 265*, 17156.
Farah, C. S., Miyamoto, C. A., Ramos, C. H. I., da Silva, A. C. R., Quaggio, R. B., Fujumori, K., Smillie, L. B., & Reinach, F. C. (1994) *J. Biol. Chem. 269*, 5230.
Flicker, P. F., Phillips, G. N., Jr., & Cohen, C. (1982) *J. Mol. Biol. 162*, 485.
Gariepy, J., & Hodges, R. S. (1983) *FEBS Lett. 160*, 1.
Glatter, O. (1982) in *Small Angle X-ray Scattering* (Glatter, O., & Kratky, O., Eds.) Chapter 4, Academic Press, New York.
Grabarek, Z., Drabikowski, W., Leavis, P. C., Rosefeld, R. S., & Gergely, J. (1981) *J. Biol. Chem. 256*, 13121.
Heidorn, D. B., & Trewhella, J. (1988) *Biochemistry 27*, 909.
Heidorn, D. B., Seeger, P. A., Rokop, S. E., Blumenthal, D. K., Means, A. R., Crespi, H., & Trewhalla, J. (1989) *Biochemistry 28*, 6757.
Henderson, S. J., Newsholme, P., Heidorn, D. B., Mitchell, R., Seeger, P. A., Walsh, D. A., Trewhella, J. (1992) *Biochemistry 31*, 437.
Herzberg, O., & James, M. N. G. (1985) *Nature (London) 313*, 653.
Herzberg, O., Moult, J., & James, M. N. G. (1986) *J. Biol. Chem. 261*, 2638.
Hjelm, R. P. (1988) *J. Appl. Crystallogr. 21*, 618.
Hubbard, S. R., Hodgson, K. O., & Doniach, S. (1988) *J. Biol. Chem. 263*, 4151.
Ibel, K., & Struhrmann, H. B. (1975) *J. Mol. Biol. 93*, 255.
Ikura, M., Clore, G. M., Gronenborn, A. M., Zhu, G., Klee, C. B., & Bax, A. (1992) *Science 256*, 632.
Kataoka, M., Head, J. F., Seaton, B. A., & Engelman, D. M. (1989) *Proc. Natl. Acad. Sci. U.S.A. 86*, 6944.
Kataoka, M., Head, J. F., Voherr, T., Krebs, J., & Carafoli, E. (1991) *Biochemistry 30*, 6247.
Kobyashi, T., Tao, T., Grabarek, Z., Gergely, J., & Collins, J. H. (1991) *J. Biol. Chem. 266*, 13746.
Kretsinger, R. H. (1980) *CRC Crit. Rev. Biochem. 8*, 119.
Kringbaum, W. R., & Kugler, F. R. (1970) *Biochemistry 9*, 1216.
Laporte, D. C., Wierman, B. M., & Storm, D. R. (1980) *Biochemistry 19*, 3814.
Leavis, P. C., & Gergely, J. (1984) *CRC Crit. Rev. Biochem. 16*, 235.
Meador, W. E., Means, A. R., & Quiocho, F. A. (1992) *Science 257*, 1251.
Meador, W. E., Means, A. R., & Quiocho, F. A. (1993) *Science 262*, 1718.
Moore, P. B. (1980) *J. Appl. Crystallogr. 13*, 168.
Moore, P. B. (1981) *J. Appl. Crystallogr. 14*, 237.
Ngai, S.-M., & Hodges, R. S. (1992) *J. Biol. Chem. 267*, 15715.
Olah, G. A., Mitchell, R. D., Sosnick, T. R., Walsh, D. A., & Trewhalla, J. (1993) *Biochemistry 32*, 3659.
O'Neil, K. T., & DeGrado, W. F. (1989) *Proteins: Struct., Funct., Genet. 6*, 284.
Pickett-Giess, C. A., & Walsh, D. A. (1986) *Enzymes (3rd Ed.) 264*, 396.
Seeger, P. A., Hjelm, R. P., & Nutter, M. J. (1990) *Mol. Cryst. Liq. Cryst. 108A*, 101.
Sundaralingam, M., Bergstrom, R., Strasbourg, G., Rao, S. T., Roychowdhury, Greaser, M., & Wang, B. C. (1985) *Science 227*, 945.
Swenson, & Frederickson (1992) *Biochemistry 31*, 3420.
Syska, H., Wilkinson, J. M., Grand, J. A., & Perry, S. V. (1976) *Biochem. J. 153*, 375.
Talbot, J. A., & Hodges, R. S. (1981) *J. Biol. Chem. 256*, 2798.
Trewhalla, J., Blumenthal, D. K., Rokop, S. E., & Seeger, P. A. (1990) *Biochemistry 29*, 9316.
Van Eyk, J. E., & Hodges, R. S. (1988) *J. Biol. Chem. 263*, 1726.
Wang, C.-L. A., Zhan, Q., Tao, T., & Gergely, J. (1987) *J. Biol. Chem. 262*, 9636.
White, S. P., Cohen, C., & Phillips, G. N., Jr. (1987) *Nature 325*, 826.
Wilkinson & Grand (1975) *Biochem. J. 149*, 493.
Wilkinson & Grand (1978) *Nature 271*, 31.
Wylie, D. C., & Vanaman, T. C. (1988) in *Molecular Aspects of Cellular Regulation* (Cohen, P., & Klee, C. B., Eds.) Vol. 5, pp 1–15, Elsevier, Amsterdam.
Xu, G.-Q., & Hitchcock-Degregori, S. E. (1988) *J. Biol. Chem. 263*, 13962.
Yoshino, H., Minari, O., & Matsushima, N. (1989) *J. Biol. Chem. 264*, 19706.
Zot, A. S., & Potter, J. D. (1987) *Annu. Rev. Biophys. Biophys. Chem. 16*, 535.